Aerospace Science and Technology 114 (2021) 106747

Contents lists available at ScienceDirect

Aerospace Science and Technology

www.elsevier.com/locate/aescte

Flow and aeroacoustic attributes of highly-heated transitional rectangular supersonic jets

Song Chen [a,*], Romain Gojon [b], Mihai Mihaescu [a]

[a] KTH Royal Institute of Technology, FLOW, 10044, Stockholm, Sweden
[b] ISAE-SUPAERO, Université de Toulouse, 31400, Toulouse, France

ARTICLE INFO

Article history:
Received 13 July 2020
Received in revised form 31 January 2021
Accepted 14 April 2021
Available online 27 April 2021
Communicated by Craig Johansen

Keywords:
Supersonic jet
LES
Aeroacoustic
High temperature
Shock wave

ABSTRACT

Heated transitional supersonic jets exhausting from a rectangular nozzle at over-expanded conditions are investigated by Large Eddy Simulations and Ffowcs-Williams and Hawkings acoustic analogy. Four cases with a fixed nozzle pressure ratio but different temperature ratios (TR) of 1.0, 2.0, 4.0, and 7.0 are analyzed. Numerical results show that with the increasing temperature the jet velocity significantly increases, whereas its Reynolds number decreases by about one order of magnitude, which leads to a 30% decrease in the jet potential core length and reduction in the number of shock cells. The increasing temperatures also result in supersonic shear layer convection Mach numbers and consequently Mach wave radiations in the acoustic fields. Pressure skewness and kurtosis factors indicate crackle noise and non-linear propagation effects in high temperatures. For the most heated jet TR 7.0, the Mach wave radiation is identified radiating noise at about 120 degrees, while the large turbulence structure noise at about 150 degrees. Furthermore, the vortex sheet model analysis and the LES data detect the existence of upstream-propagating neutral waves inside jet TR 7.0. The observed screech frequency falls within the range of antisymmetric mode indicating that the highly-heated jet is characterized by an antisymmetric oscillation mode at the screech frequency.

1. Introduction

Rectangular nozzles, as compared with their axisymmetric opponents, are more suitable for future high-speed aircraft for several attractive features, e.g., reduction of the aerodynamic drag due to better integration to the airframe, ease of design and manufacture as relatively fewer components needed for the thrust vector control [1,2], and improved entrainment and mixing performance of the exhausting jet [3,4]. Among many aspects of jet research, supersonic jet noise has been a topic of increasing interest for the past several decades [5–7].

Main components that contribute to the supersonic jet noise include turbulent mixing noise, Mach wave radiation, broadband shock-associated noise (BBSAN), and screech noise [8–11]. The turbulent mixing noise is generated by both the large turbulent coherent structures and the fine-scale turbulence in the shear layer. Fully turbulent jets have one strong acoustic source near the end of potential core and laminar jets are characterized by strong vortex pairing noise mainly radiating from the nozzle exit. In comparison, transitional jets that have transitional shear layers with turbulent fluctuations emit noise from different locations depending on the shear layer thickness and fluctuation levels [12–14]. For a supersonic jet, large turbulent scales dominate and radiate the mixing noise into an angular sector of about 140 ∼ 160 degrees measured from the jet upstream direction. The Mach wave radiation is a unique component of supersonic jet that can be explained by the wavy wall analogy [8]. In this analogy, large-scale turbulent structures of shear layers are treated as wavy walls. The wavy wall travels downstream at a supersonic speed so that compression/Mach waves are generated. The directivity of this noise component can be estimated by using the convection Mach number. The BBSAN, first identified by Harper-Bourne and Fisher [15], is generated by the interactions between a quasi-periodic shock cell structure in the jet core and turbulent flow structures in the jet shear layer. The screech noise, first observed by Powell [16,17], is characterized by strong and discrete tones. This noise component is generated by an aeroacoustic feedback mechanism in the mixing layer which includes both downstream convected turbulent vortical structures from the lip of nozzle and upstream propagating acoustic waves generated by the interaction of perturbations with shock cells. Screech tones are primarily radiated in the upstream direction.

* Corresponding author, presently at the Centre for Climate Research Singapore, 537054 Singapore.
E-mail address: sonc@mech.kth.se (S. Chen).

https://doi.org/10.1016/j.ast.2021.106747

Current noise reduction techniques, such as fluidic injection and chevrons [18–20], are developed mainly based on low-temperature laboratory-scale jet data. However, the total temperature of a practical jet applied to future civil supersonic flights and present military aircraft engines can be higher than 2000 K. There is thus a crucial need to understand the high-temperature effects on the supersonic jet. Both experimental and computational efforts are needed to obtain insights into the flow fields and the noise generation mechanisms in the high-temperature regime. The current laboratory-scale experiments have achieved a nozzle temperature ratio (TR = T_t/T_∞, where subscripts t and ∞ mean total and ambient conditions) of 3.0, which corresponds to a total temperature of 900 K [21–24]. However, this is far below the typical temperature in realistic scenarios.

A few studies have addressed general temperature effects on jets. Tam et al. [25,26] reported that jet noise can be affected by hot temperatures from two perspectives: a large density gradient and an increased convection Mach number. The large density gradient in a hot jet has a strong influence on both the mean flow and the turbulent mixing noise. When the jet is heated, the density difference between the jet and the ambient tends to enhance the Kelvin-Helmholtz instability [27]. This promotes the turbulent mixing as well as the jet spreading rate. However, the increased convection Mach number in hot jets tends to stabilize the turbulent mixing [28], which may counterbalance the density gradient effect to some extent. Compared with cold jets, hot ones have a shorter eddy decay time and slightly reduced eddy size which may affect noise radiations [29]. Viswanathan [30] studied the effect of jet temperature on the noise radiation but in subsonic jets. The Reynolds number was found to impact the shape of the noise spectrum; however, when the Reynolds number exceeds 4.0×10^5, its effect on acoustic characteristics can almost be neglected [30]. Among numerical works on hot supersonic jets, Cacqueray and Bogey [31] and Langenais et al. [32] analyzed supersonic jets with a total temperature around 1100 K and identified strong non-linear effects resulting in series of N-shaped waves. Gojon et al. [33,34] investigated the temperature effects (up to 900 K) on the aerodynamic and acoustic fields of a rectangular supersonic jet using LES. The pressure spectra showed an intensified screech feedback mechanism when the temperature was increased. Nonomura et al. [14] studied a hot supersonic jet around 1200 K by using LES and found stronger Mach waves emitted at wider radiation angles. Liu et al. [35–37] conducted studies on the aeroacoustic characteristics of highly heated round supersonic jets with TR up to 7.0. A temperature-dependent specific heat ratio was found to be important for accurately capturing the noise prediction in high temperatures. Except for the works of Liu et al. [35–37], highly-heated jets with temperature around 2000 K have not received much attention. In the far-field acoustic spectra, cold subsonic/supersonic jets only display a single downstream lobe close to the jet plume, which is caused by the turbulent mixing noise at about at $140 \sim 160$ degrees. However, the highly-heated jets showed an interesting dual-lobe pattern in the frequency spectra: one close to the jet plume at $140 \sim 160$ degrees and the other at $115 \sim 120$ degrees [35]. Liu et al. [35] claimed the one at $115 \sim 120$ degrees was attributed to Mach wave radiation. A similar pattern in the frequency spectra was also reported by Tam and Parrish [38] in analyzing the noise data of a F-22A Raptor. They suspected, however, the new component at $115 \sim 120$ degrees might be the indirect combustion noise generated by entropy waves coming out of the afterburner [38]. Further studies on the highly-heated jets for an enhanced understanding of the noise generation mechanisms are thus highly needed. Furthermore, studies on the rectangular shape jets for future civil supersonic flights and high-performance jet engines, have scarcely been reported in literature.

Table 1
Nozzle operating conditions.

Case	NPR	TR	M_j	$u_j(m/s)$	$T_j(K)$	M_a	Re
JetTR1	3.0	1.0	1.36	399	214	1.17	9.61×10^5
JetTR2	3.0	2.0	1.36	564	430	1.66	3.96×10^5
JetTR4	3.0	4.0	1.37	801	888	2.36	1.67×10^5
JetTR7	3.0	7.0	1.39	1070	1607	3.15	0.85×10^5

In light of the above, the current study targets to fill this research gap by investigating the highly-heated transitional rectangular supersonic jet using the LES approach. The focus is on the high temperature effects up to TR 7.0, especially on rectangular jets. This paper is organized in the following way: section 2 describes the nozzle geometry and operating conditions; flow solver and numerical methods are given in section 3; the numerical results and the analysis are presented in section 4 and 5, and section 6 summarizes and concludes the findings.

2. Nozzle geometry and operating conditions

A convergent-divergent (C-D) rectangular nozzle previously studied by Gojon et al. [33,34,39] and tested at the University of Cincinnati [21,22,40,41] is selected for this work. The rectangular nozzle has an aspect ratio of 2.0 with a C-D profile on the minor axis plane and a constant width on the major axis plane. It has a design Mach number of 1.5 at nozzle pressure ratio (NPR = P_t/P_∞, where subscripts t and ∞ mean total and ambient conditions) 3.67 and TR 1.0. Different from a smooth contoured nozzle, the current one has a sharp throat. A set of shock waves is thus expected from the tip corner inside the nozzle. Detailed information about the nozzle geometry and operating conditions are available in Refs. [21,22]. In this study, a slightly over-expanded condition with an NPR of 3.0 is selected with four different TRs (i.e. 1.0, 2.0, 4.0, and 7.0). The ambient pressure and temperature are p_∞=101325 Pa and T_∞=293 K. The four cases are referred to as JetTR1, JetTR2, JetTR4, and JetTR7 respectively.

The maximum total temperature of the jet reaches about 2100 K. In high temperatures, air starts to dissociate and its composition changes. This can affect the properties of gaseous mixture significantly (e.g., the specific heat ratio γ) as well as the flow and acoustic fields. When temperature increases from 300 K to 2000 K, γ of air drops from 1.4 to 1.27 [42]. Based on Liu et al. [37], a temperature-dependent specific heat ratio γ is recommended for accurately simulating the highly-heated jets. In this work, the chemical reactions involved in the air dissociation process within the high-temperature range are neglected during the LES simulations for simplicity. However, the temperature-dependent and species-dependent thermodynamic properties of air are considered by introducing a table pre-calculated by the chemical equilibrium computation [43].

Details of the nozzle operating conditions are shown in Table 1. One can see the ideally expanded Mach number M_j slightly changed with the temperature ratio due to the change of γ at high temperatures. The ideally expanded jet velocity u_j and static temperature T_j increase significantly. The acoustic Mach number, defined as the ratio of the flow speed and the ambient speed of sound $M_a = u_j/\sqrt{\gamma R T_\infty}$, is amplified by about 3 times from JetTR1 to JetTR7. The Reynolds number, Re, decreases dramatically due to the greatly elevated kinematic viscosity at high temperatures. It is defined as $(u_j D_{eq})/\nu(T)$, where u_j denotes the ideally expanded jet velocity, D_{eq} is the jet equivalent diameter, and $\nu(T)$ is the temperature-dependent kinematic viscosity. The equivalent diameter D_{eq} is computed by converting the rectangular nozzle into a round nozzle with the same exit area. Kinematic viscosity can be expressed as the ratio of dynamic viscosity to density

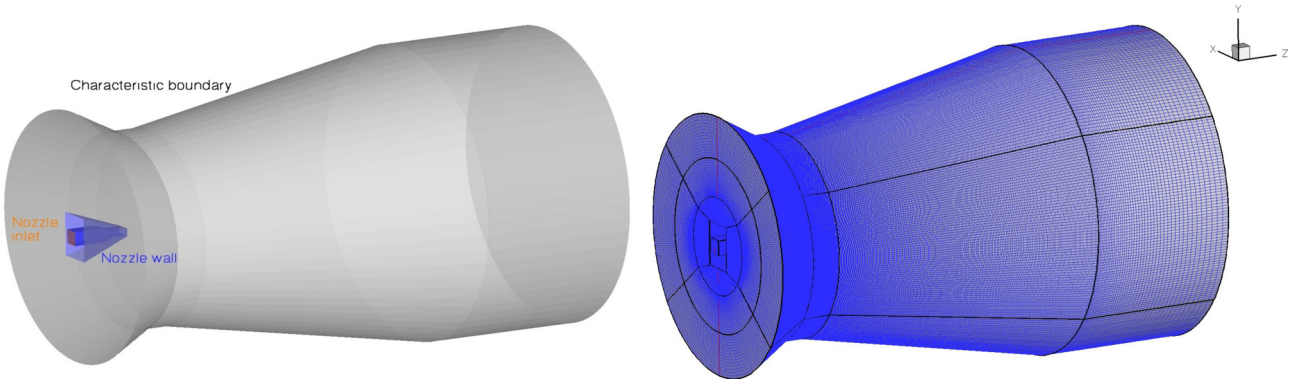

Fig. 1. Schematic of the computational domain (left) and the multi-block grid (right).

$\nu(T) = \mu(T)/\rho(T)$, where dynamic viscosity increases and density decreases at high temperatures. The temperature-dependent dynamic viscosity $\mu(T)$ is estimated by Sutherland's formula [44].

3. Computational methodology

3.1. Numerical methods

Simulations are performed using a compressible finite-volume based flow solver [45] that has been validated in previous studies by Semlitsch et al. [46] and Gojon et al. [33,34,39]. Good agreements of flow and acoustic fields between the CFD prediction and experimental data are achieved. An implicit LES method [47] or monotonically integrated large eddy simulation (MILES) [48] is adopted in which the small scales are represented implicitly by the numerical dissipation. Explicit standard four-stage Runge-Kutta algorithm is applied for time integration and a second-order central difference scheme is used for spatial discretization. A Jameson-type [49] artificial dissipation is implemented to handle the subgrid scales and to capture shocks. Details of the artificial dissipation term can be found in the work of Gojon et al. [33].

3.2. Computational domain and boundary conditions

The cylindrical computational domain encloses the rectangular nozzle and the ambient area surrounding the downstream jet plume. In the jet streamwise direction, the length of the enclosing domain is around $67h$, where h is the nozzle height in the minor axis plane. In the radial direction, the radius of the domain is about $21h$. Total pressure and total temperature are employed at the nozzle inlet. Adiabatic non-slip conditions are applied at the nozzle wall. Non-reflecting boundary conditions using invariants are used at the surrounding boundaries, where the ambient static pressure and temperature are imposed. Moreover, in order to avoid spurious sound reflections from those boundaries, sponge zones (i.e. about $10h$ in the radial direction) are added in the computational domain. It should be noted that different from experimental fully turbulent jets, the current inflow boundary condition yields a laminar flow at the inlet. Through developing inside the nozzle and disturbed by internal shock waves, a transitional jet is formed at the nozzle exit.

The computational grid is a multi-block structured mesh consisting of about 160 million cells as shown in Fig. 1. It has been evaluated in our previous grid-convergence study [33]. Grid points are clustered in the jet region where large flow gradients exist, and it is stretched slowly in both the axial and radial directions. The grid resolution near the nozzle wall has a dimensionless distance $y^+ \sim 1$. In the wall parallel directions both x^+ and z^+ are less than 10. The growth ratio of the grid is controlled below 5% to avoid high dissipation or dispersion errors from the spatial derivation scheme.

Computations are performed on 960 processors. A time step of $\sim 0.002h/u_j$ is used during the simulations, which corresponds to $1.0 \times 10^{-7}s$ for JetTR1 and $3.0 \times 10^{-8}s$ for JetTR7. After about 8 convective times (roughly the jet transient state), time-history data on points and surfaces are saved and statistics are computed over 32 convective times. The total computational time for the cold jet JetTR1 is about 240,000 core hours. For the cases with a higher temperature, the time step becomes smaller due to the increased u_j. The overall computational time for hot jets is thus further increased to reach the same physical time as for the cold jet scenario.

The current work is a continuation of our previous work [33,34], where the detailed grid convergence study and verification and validation of numerical methods are reported. Cases tested include the acoustic pulse, shock propagation, and shock-vortex interaction. The numerical method has also been used to study the supersonic jet with relatively low temperature ratios, and results match well with the experiments conducted at the University of Cincinnati [22]. Interested readers can refer to [33,34] for details.

4. Aerodynamic results and discussions

4.1. Instantaneous fields

Snapshots of static temperature contours are presented in Fig. 2. When the flow goes through the C-D nozzle, it is accelerated from subsonic to supersonic. Flow static temperature decreases due to the flow acceleration. The temperature evolution inside the nozzle in each case can be observed in Fig. 2. Shock structures within the nozzle and the jet core region are also visible in the temperature contours. Due to the sharp corner of the nozzle throat, oblique shocks are formed. They are reflected by the nozzle wall and hit the nozzle lip. When the over-expanded jet flows out of the nozzle, another set of shock wave is generated from the nozzle lip. It merges with the internally reflected shock waves generated from the nozzle throat and forms shock diamonds inside the jet core. All cases have a transitional shear layer at the nozzle exit, i.e. the shear layers in the nozzles are mainly laminar, but some turbulent fluctuations are already present in the flow. Those fluctuations, visible in Fig. 15, permit to avoid having a pairing noise in the simulations. The transitional shear layers provoke fast growing Kelvin-Helmholtz instabilities that promote the mixing of the jet and the ambient air. These initial flow instabilities, developed in the jet shear-layer close to the nozzle lip, evolve rapidly into chaotic motions downstream.

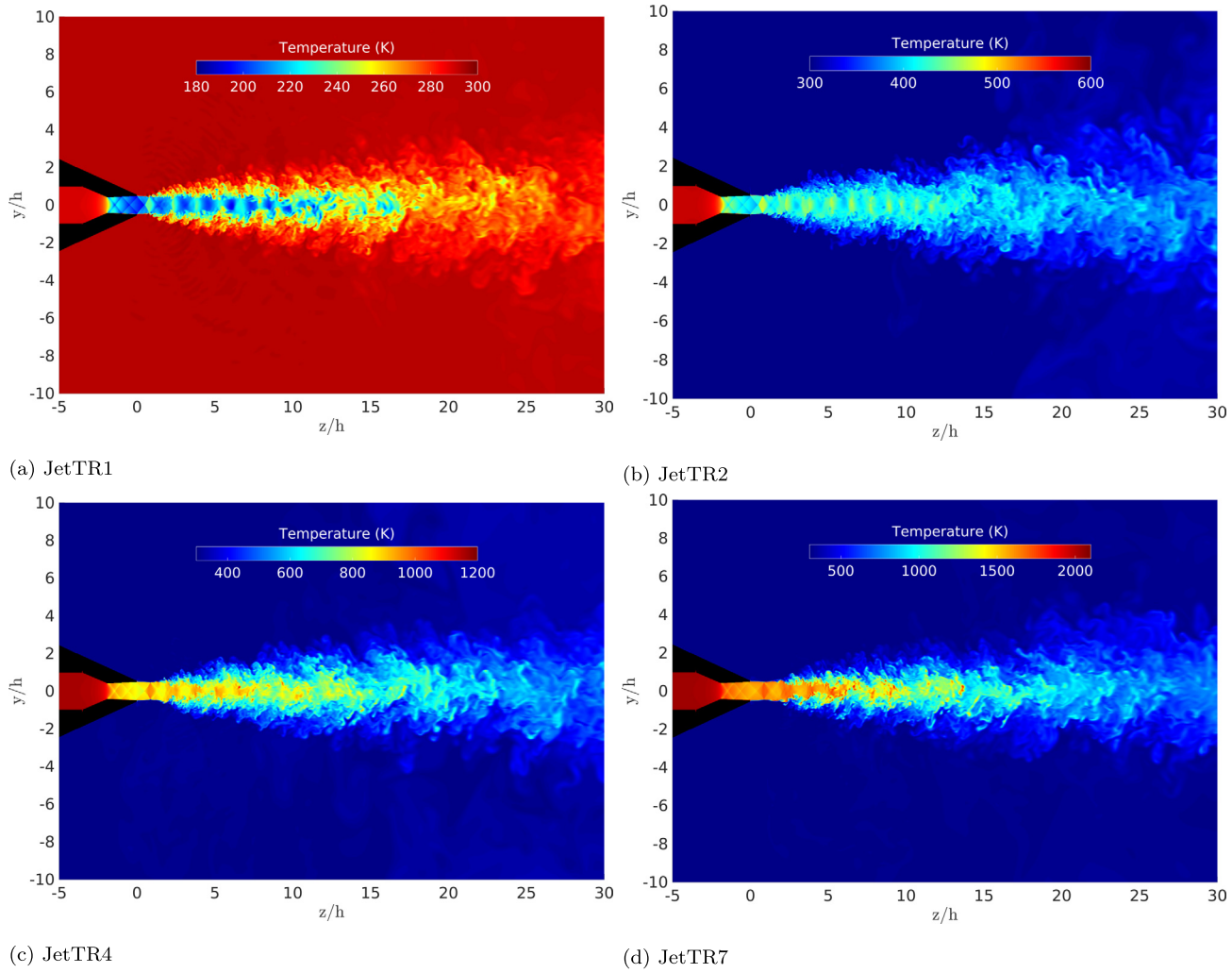

(a) JetTR1 (b) JetTR2

(c) JetTR4 (d) JetTR7

Fig. 2. Instantaneous fields of static temperature in the minor axis plane. The nozzle is in black.

4.2. Time-averaged flow fields

Properties of the jet mean flow fields are studied. Fig. 3 shows the mean axial velocity in both the minor and major axis planes normalized by the ideally expanded jet velocity u_j. According to the value of u_j in Table 1, it can be known that the magnitude of jet exit velocity is increased significantly for hot jets. The length of the potential jet core decreases rapidly in hot jets. The core length of JetTR1 configuration as shown in Fig. 3a is slightly larger than $z/h = 15$, whereas the length of JetTR7 is as short as $z/h = 10$ as shown in Fig. 3d. There is around 30% reduction in the jet potential core length. This is mainly due to the reduced Reynolds number effect as a hot jet has a greatly increased kinematic viscosity and thus higher viscous dissipations. Moreover, the number of shock cells inside the jet core is reduced significantly too.

Convection velocity and convection Mach number of the shear layer turbulent structures are associated with the Mach wave radiation component. Convection velocities of the shear layers in both the minor and major axis planes are computed using cross-correlations of axial velocity fluctuations. Results are shown in Table 2 and plotted in Fig. 4 along the axial direction. Normalized convection velocities, u_c/u_j, in the minor and major axis planes are shown in Figs. 4a and 4c. Convection Mach numbers, $M_c = u_c/a_\infty$, in the minor and major axis planes are shown in Figs. 4b and 4d. Zigzag plots in Fig. 4 indicate that the vortical structures in the shear layer experience decelerations and accelerations associated with the presence of shock waves and expansion waves in the shock cell structure of the jet.

Table 2
Jet shear layer properties: LES $\overline{u_c/u_j}$ and LES $\overline{M_c}$ are the normalized average convection velocity and convection Mach number computed from the simulation data in the minor axis plane between $z = 2h$ and $z = 5h$.

Case	TR	$u_j(m/s)$	$T_j(K)$	$a_j(m/s)$	LES $\overline{u_c/u_j}$	LES $\overline{M_c}$
JetTR1	1.0	399	214	293	0.77	0.95
JetTR2	2.0	564	430	415	0.70	1.24
JetTR4	4.0	801	888	586	0.62	1.60
JetTR7	7.0	1070	1607	774	0.56	1.88

In Figs. 4a and 4c, the normalized convection velocity decreases when the jet temperature rises. However, the convection Mach number exhibits the opposite trend. The averaged convection Mach number, $\overline{Mc}$, as listed in Table 2, can represent the convection speed of large turbulent structures in the wavy wall analogy. It can be used to estimate the directivity of Mach wave radiation that will be discussed later. Apart from JetTR1 with a subsonic acoustic convection Mach number 0.95 as shown in Table 2, all the other three cases have a supersonic convection Mach number. Furthermore, the convection Mach numbers in the major axis plane are smaller than those in the minor plane from Figs. 4b and 4d. This suggests different Mach wave radiation angles in the two different planes.

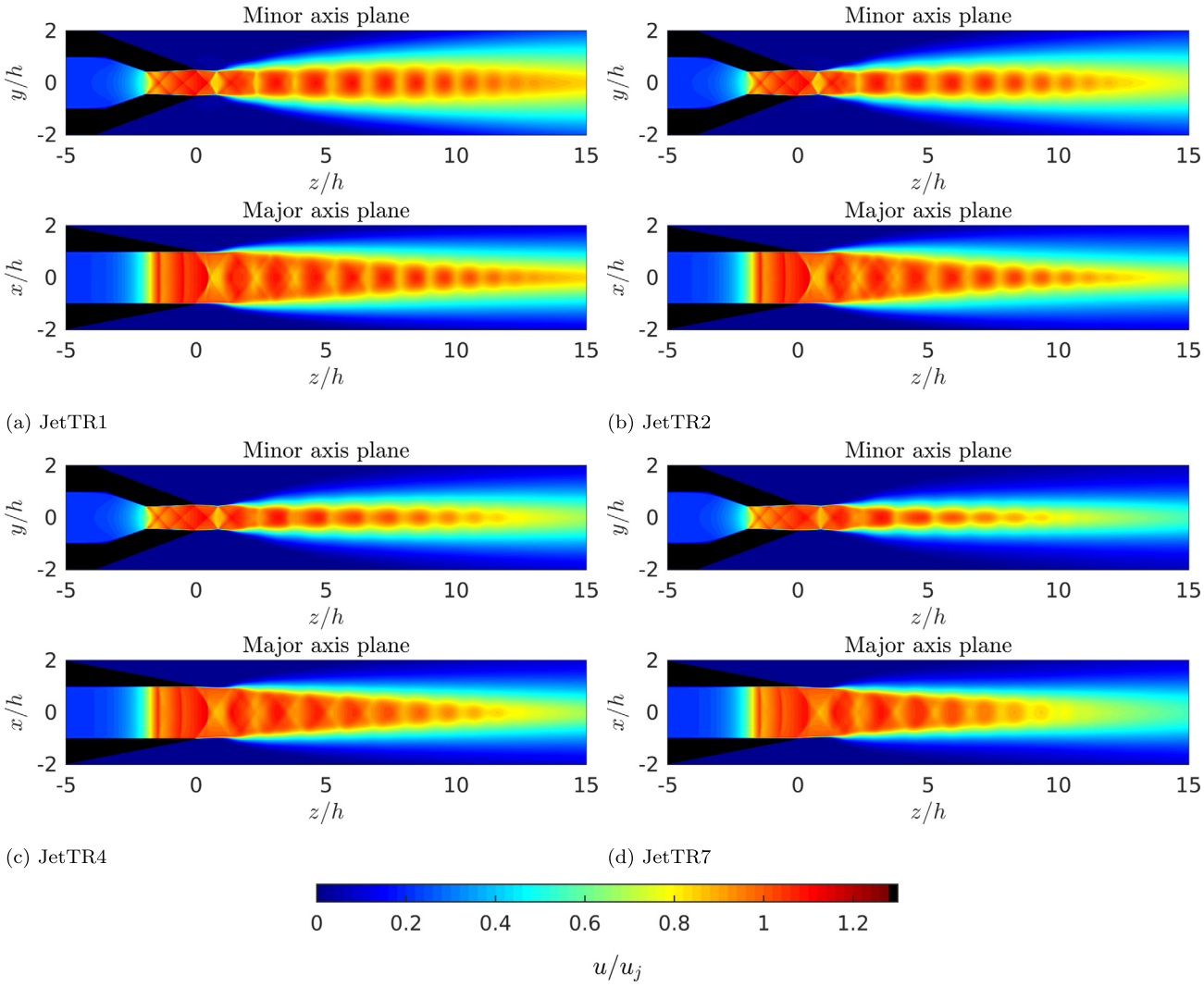

Fig. 3. Mean axial velocity fields normalized by the corresponding ideally expanded jet velocity u_j.

5. Acoustic results and discussions

5.1. Near-field data

OASPLs obtained at the minor and major axis planes near the jet are shown in Fig. 5. They are amplified in all directions when the jet temperature increases. Another feature is that the Mach wave radiation component at about 120 degrees measured from the jet upstream direction becomes much significant in hot jets. Meanwhile, one can observe that the Mach wave radiation in the minor axis plane has higher amplitudes than those in the major axis plane. One should note that the strong Mach wave radiation is one of the characteristics of transitional jets. The laminar shear layer rolls up and forms large turbulent structures during transition. These vortex pairing [12] traveling at supersonic speeds generates stronger Mach wave radiation than a fully turbulent jet does [14].

Pressure spectra obtained in the vicinity of the nozzle at $(x/h, y/h, z/h) = (0, 2, -2)$ are shown in Fig. 6 as a function of the Strouhal number $St = f D_{eq}/u_j$. There is a dominant frequency for each jet at Strouhal number ranging from 0.25 to 0.38, as shown in Table 3. These dominant frequencies represent screech tones. Except for JetTR2, no visible harmonic frequencies of the screech tone are found. When the jet temperature increases, the amplitude of this screech component first increases from 150 dB/St for JetTR1, to 159 dB/St for JetTR2, to 162 dB/St for JetTR4, and to 162.5 dB/St for JetTR7. In the work of Mora et al. [22], however, they found an overall decrease in the amplitude of the screech when the jet TR increased up to 3.0. We suspect that this disagreement on screech may be due to the transitional nature of jets in the study, while fully turbulent jets are tested in the experiments. Different initial shear layers (i.e. laminar or turbulent) have a direct impact on the feedback loop of the screech.

Tam [50] proposed a model to predict the screech frequency for rectangular and non-axisymmetric jets. For rectangular nozzles, it can be expressed as:

$$St_{Tam} = \frac{\frac{D_{eq}u_c/u_j}{2h(1+u_c/a_\infty)(M_j^2-1)^{1/2}}[(h_j/b_j)^2+1]^{1/2}}{\left\{\left[\frac{1+\frac{\gamma-1}{2}M_j^2}{1+\frac{\gamma-1}{2}M_d^2}\right]^{(\gamma+1)/(2(\gamma-1))}\frac{M_d}{M_j}-1\right\}\frac{b}{b+h}+1} \quad (1)$$

where h and b are the height and width of the rectangular jet at the exit plane, h_j and b_j are the height and width of the ideally expanded jet [50], M_d stands for the nozzle design Mach number, and M_j is the ideally expanded jet Mach number. Taking the variable γ into account, the computed values using Eq. (1) are listed in Table 3. For comparison, the experimental results of the screech tones for JetTR1 and JetTR2 are also included. It can be seen that the screech frequency $St_{screech}$ predicted by the simula-

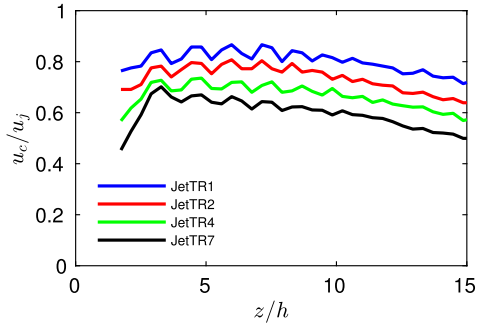

(a) Normalized convection velocity, minor axis plane

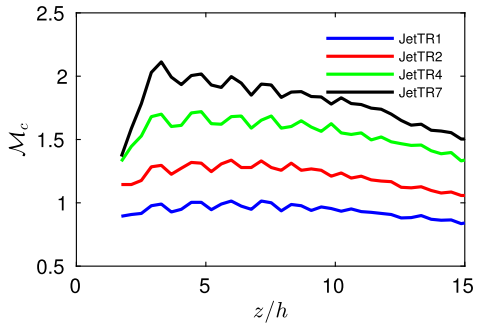

(b) Convection Mach number, minor axis plane

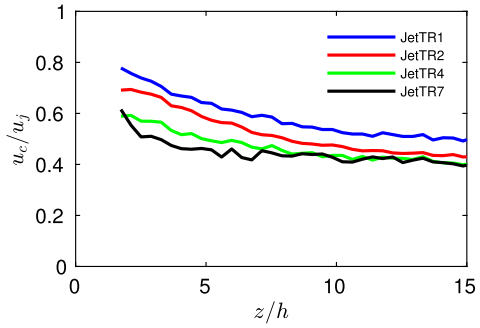

(c) Normalized convection velocity, major axis plane

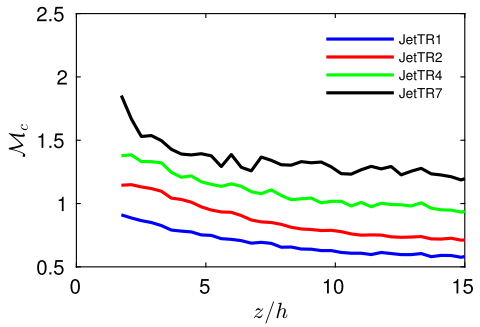

(d) Convection Mach number, major axis plane

Fig. 4. Normalized convection velocity (a, c) and convection Mach number (b, d) of the turbulent structures in the jet shear layer.

Table 3
Peak values for the pressure spectra at $(x, y, z) = (0, 2h, -2h)$. $St_{screech}$ and $dB_{screech}$ are the Strouhal number and the sound pressure level at the peak.

Case	TR	$St_{screech}$	$dB_{screech}$	$St_{screech}$ exp.	St_{Tam}
JetTR1	1.0	0.38	150	0.37	0.39
JetTR2	2.0	0.31	159	0.31	0.32
JetTR4	4.0	0.26	162	–	0.26
JetTR7	7.0	0.25	162.5	–	0.21

tion results agrees well with the experimental data. Tam's formula also provides good estimations for jets with a TR up to 4.0. For the highly-heated jet JetTR7, a 15% difference between the LES data and the theoretical prediction exists.

5.2. Mach wave radiation

Mach wave radiation is a unique noise component of supersonic jets. It is generated by large-scale turbulent structures in the jet shear layer convected downstream at supersonic speeds. Its directivity is closely related to the convection Mach number. Pressure fluctuation contours in Fig. 7 illustrate the Mach wave radiation in both the minor and major axis planes. For the cold jet in Figs. 7a and 7b, there is no obvious Mach wave radiation. This is consistent with the subsonic convection Mach number found in the previous subsection. When the jet temperature ratio increases to 2.0 and 4.0, this noise component emerges by strong pressure fluctuations at about 140 degrees in both the minor and major axis planes. When the jet temperature increases to 7.0 as shown in Figs. 7g and 7h, the Mach waves become more significant compared with cold ones. Similar to Fig. 5, the minor axis plane also shows a stronger Mach wave radiation than the major axis plane, due to the stronger turbulent kinetic energy caused by the shock and shear layer interactions in the minor axis plane.

Jet temperature affects the directivity of Mach wave radiation. When the jet temperature increases from TR = 2.0 to TR = 7.0, Fig. 7 shows that the propagation direction inclines towards the sideline direction. This difference can be observed from the pressure contours directly or by checking the white lines indicating the propagation direction in Figs. 7c, 7e, and 7g. The Mach wave radiation directivity can be estimated by the convection Mach number, M_c. If the angle is measured from the upstream direction, the formula can be expressed as [51]:

$$\theta = 180 - arccos(\frac{1}{M_c}) \tag{2}$$

Using the averaged convection Mach number $\overline{M}_c$ from Table 2, the propagation direction angle can be estimated by Eq. (2). Noted again that $\overline{M}_c$ for JetTR1 is subsonic, 0.95, which explains why there is no Mach wave radiation observed in Figs. 7a and 7b. For the other three cases, the calculated Mach wave radiation angles are 144, 129, and 122 degrees respectively. The smaller propagation angle of 122 degrees for JetTR7 indicates a Mach wave radiation inclining more towards the sideline direction, which is consistent with the results shown in the contours. In Figs. 7c, 7e, and 7g, these estimated angles are plotted by white lines.

For heated supersonic jets, crackle noise first investigated by Ffowcs Williams et al. [52] may occur. This noise component is characterized by intermittent positive pressure spikes with a strong compression followed by a gradual expansion [53]. Crackle noise propagates downstream along the Mach wave radiation direction and may account for as much as 30% of the overall sound pressure levels in this direction [54,55]. There are two parameters commonly used to identify the crackle noise. The first one is skewness of pressure signals [53]. It is defined as:

$$S = \frac{E[(p(t) - \overline{p(t)})^3]}{\sigma^3} \tag{3}$$

where E stands for the expected value, $p(t)$ and $\overline{p(t)}$ are pressure signal and its mean value, σ denotes the standard deviation of the

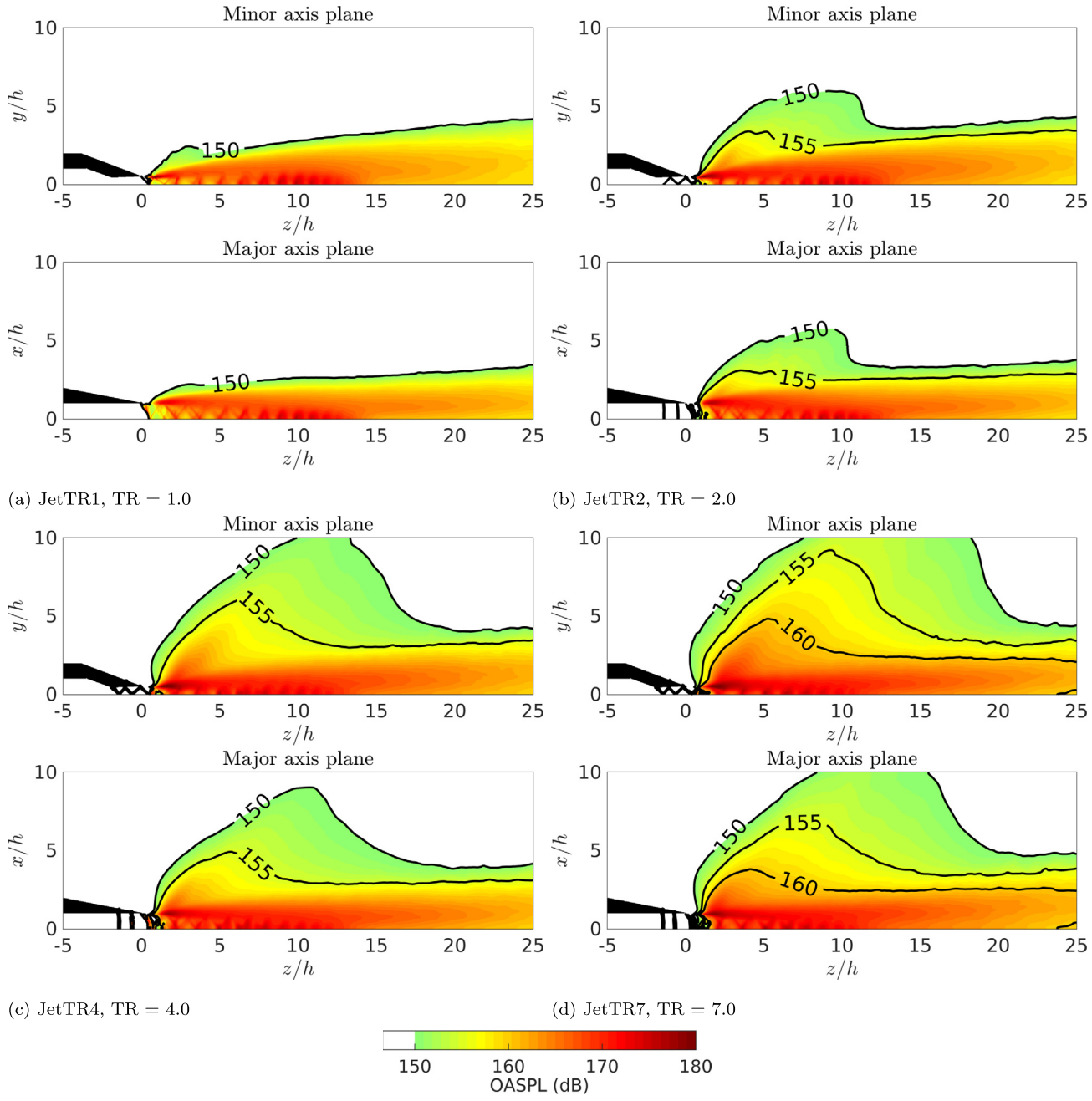

Fig. 5. Near field overall sound pressure level (OASPL).

pressure signal. When applying to acoustic signals, the skewness is a measure of asymmetry between the crest and trough of an acoustic wave. If the skewness exceeds 0.4, it indicates that the crackle noise component exists, while there is no crackle noise if the skewness is smaller than 0.3 [53]. Another statistical parameter is kurtosis [56], which is useful for evaluating the crackle or the nonlinear effect. The kurtosis is defined as:

$$K = \frac{E[(p(t) - \overline{p(t)})^4]}{\sigma^4} - 3 \tag{4}$$

Kurtosis is an indicator of intermittency of the wave. It quantifies the distribution of a signal compared with a Gaussian distribution. A value of zero means the shape of the signal is the same as the Gaussian distribution. A positive kurtosis indicates longer and thicker tails than the normal distribution, while a negative kurtosis indicates shorter and thinner tails. For the crackle noise or the "N-shaped" non-linear waves, the distribution differs from the Gaussian distribution and usually with a thick tail, which indicates that the intermittency of the signal is quite strong, with high-amplitude N-shaped waves observed intermittently [31,57].

A point probe is placed along the Mach wave direction, as shown in Fig. 8a, to save the time history data during the simulations. The skewness and kurtosis factors of the pressure signal at this point are calculated and plotted in Figs. 8b and 8c. Fig. 8b shows the skewness increases from 0.1 to 0.5 in hot jets. According to the threshold value of 0.4, both JetTR4 and JetTR7 contain the crackle noise component. A similar increasing trend can also be found in the kurtosis factor. JetTR1 has the minimum kurtosis value of 0.04 among the four cases. This means that the pressure signal of JetTR1 has a low intermittency and its probability density function (PDF) is close to the Gaussian distribution, as shown in Fig. 8c. Large kurtosis and skewness values in hot jets

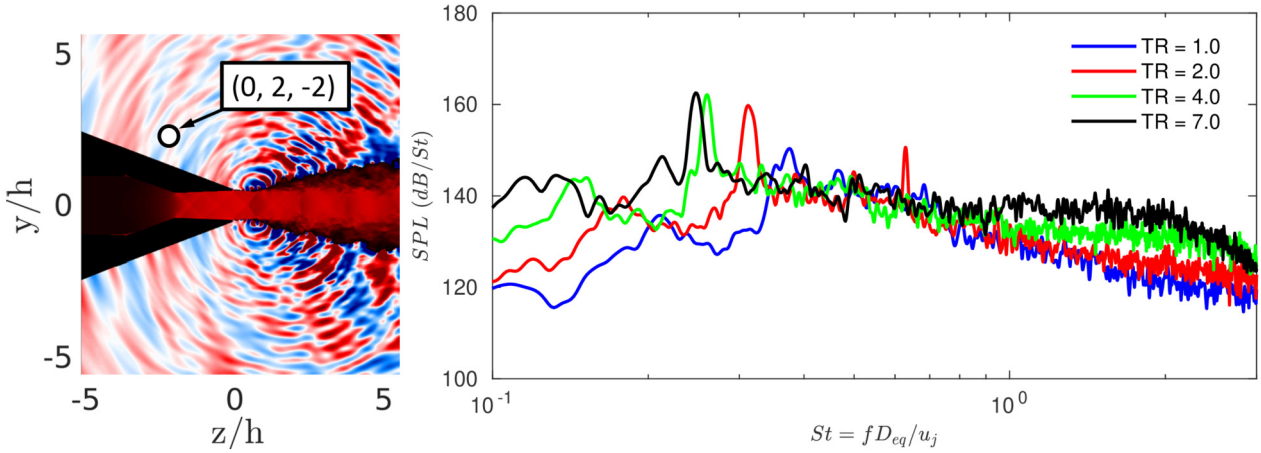

Fig. 6. Location of the point probe at $(x/h,\ y/h,\ z/h)$= (0, 2, −2) (left) and the pressure spectra for different TRs (right).

indicate high intermittency and steep pressure wave-forms. Segments of the pressure fluctuation histories for the four cases are shown in Fig. 9 and the zoomed-in pressure wave forms are presented in Fig. 10. Larger amplitudes of pressure fluctuation and amplified spikes in the wave form can be clearly seen in the high-temperature jet in Fig. 10d.

5.3. Far-field acoustic data

Far-field acoustic characteristics of the jets are studied by using the Ffowcs Williams-Hawkings (FW-H) acoustic analogy. The axisymmetric FW-H surface is illustrated in Fig. 8a by the solid black lines. OASPL at a distance of $40D_{eq}$ (the center is at the nozzle exit center) is plotted in Fig. 11 as a function of polar angle θ. For JetTR1 and JetTR2, good agreements with the experimental data were achieved and reported in [33,34]. When the jet is heated, the OASPL in the upstream direction at θ from $20 \sim 40$ degrees only shows small changes. In the sideline direction at around 90 degrees, Jet TR7 has an increase of the OASPL by 8 dB compared with the cold one. The most significant increase of OASPL is reached for an angle of θ about 120 degrees. Indeed, a difference of almost 20 dB is visible between JetTR1 and JetTR7. This dramatic increase is due to the Mach wave radiations. Moreover, the directivity angle corresponding to the peak of the Mach wave radiation slightly shifts upstream with the increase of the jet temperature, as expected. The previously estimated Mach wave radiation angles with Eq. (2) are plotted here by vertical dash lines. Good agreements with the peaks of the OASPL profiles can be seen in Fig. 11. As transitional jets, higher level of noise in the farfield are expected at all directions compared with the fully turbulent ones according to the work of Nonomura et al. [14]. This suggests the current shape of OASPL for transitional jets will be maintained in fully turbulent jets.

Fig. 12 shows the far-field acoustic spectra as a function of angle. For the cold jet in Fig. 12a, three main noise components can be observed: the screech, large turbulent structure (LTS) mixing noise, and broadband shock associated noise (BBSAN). The screech component is visible in the upstream direction at θ around $20 \sim 60$ degrees. It has a non-dimensional frequency St of 0.38. The LTS mixing noise component is characterized by a Strouhal number of about 0.2 [8] and propagates to the downstream direction at θ around $140 \sim 160$ degrees. The third component, BBSAN, is characterized by large amplitudes in SPL over a range of frequencies. Based on the work of Harper-Bourne and Fisher [15], the central frequency of BBSAN can be estimated from:

$$f_{BBSAN} = \frac{N \times u_c}{L_s(1 + M_c cos(\theta))} \tag{5}$$

where f_{BBSAN} is the central frequency of BBSAN, N denotes the mode number, u_c and M_c are the convection velocity and convection Mach number. For $N = 1$, the estimated f_{BBSAN} is illustrated by a curved black-dash line in Fig. 12.

When the jet is heated, the above mentioned three components still exist with amplified magnitudes. For the screech noise, the decrease of its frequency with the increase of the temperature of the jet is recovered here. Moreover, for the LTS noise, its frequency and radiation angle stay constant with the increase of the jet temperature whereas its amplitude increases significantly by about 10 dB between JetTR1 and JetTR7 for example. This increase is related to the increase of the jet speed and mixing with the ambient.

As it can be seen in Figs. 12b, 12c, and 12d, another noise component emerges. It corresponds to the MWR studied earlier. In the highly-heated jet this noise component peaks at about 120 degrees, while the LTS noise component peaks at about 140 ∼160 degrees. A double-peaks pattern in the noise spectra has been reported in the literature with respect to high-performance engine at afterburner conditions [35,38]. With the current LES data sets, the SPLs are analyzed for discrete frequencies (i.e. St = 0.05 and 0.5) in Fig. 13. In the low frequency regime, e.g. St = 0.05 as shown in Fig. 13a, SPL peaks are located at around 140 ∼160 degrees, which is the LTS noise as discussed above. One can see that with the increase of jet temperature, the directivity of the LTS component almost does not change. For the higher frequency St = 0.5 as shown in Fig. 13b, the SPL peak is sensitive to the temperature. Its directivity shifts from about 150 degrees in JetTR1 to about 120 degrees in JetTR7. By comparing Fig. 13a and Fig. 13b, the heated jets show two different peaks in the low-frequency (i.e. Fig. 13a) and the high-frequency (i.e. Fig. 13b) ranges. For example, in the highly-heated jet JetTR7, the dominant low-frequency component propagates to about 140 ∼160 degrees in Fig. 13a, while the dominant high-frequency component propagates to a different angle at about 120 degrees in Fig. 13b.

A possible explanation for the double-peaks pattern previously reported in [38] assumes the 120 degrees peak attributed to indirect combustion noise. Based on the current LES results without any combustion involved, this noise component would be the Mach wave radiation (MWR) generated by the large turbulent flow structures traveling at supersonic speeds. Recalling the previously estimated MWR propagation directions using the convection Mach number in the shear layer, white dashed lines representing the directivity in each case are added in Fig. 12. There is a good agreement between the estimated MWR direction and this noise com-

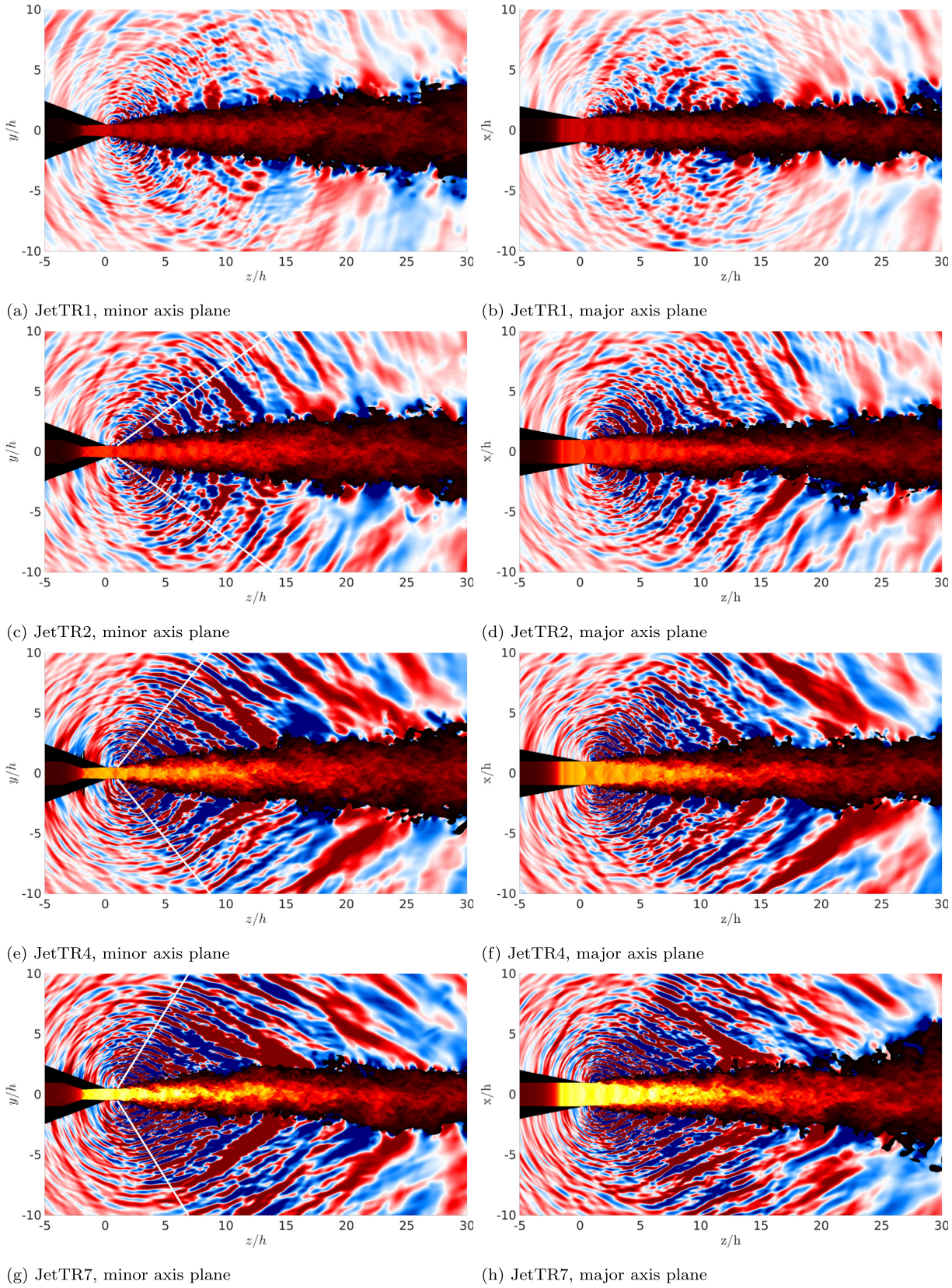

(a) JetTR1, minor axis plane

(b) JetTR1, major axis plane

(c) JetTR2, minor axis plane

(d) JetTR2, major axis plane

(e) JetTR4, minor axis plane

(f) JetTR4, major axis plane

(g) JetTR7, minor axis plane

(h) JetTR7, major axis plane

Fig. 7. Near field fluctuating pressure and jet acoustic Mach number contours. White lines show the directivity of Mach wave radiation estimated by the convection Mach numbers.

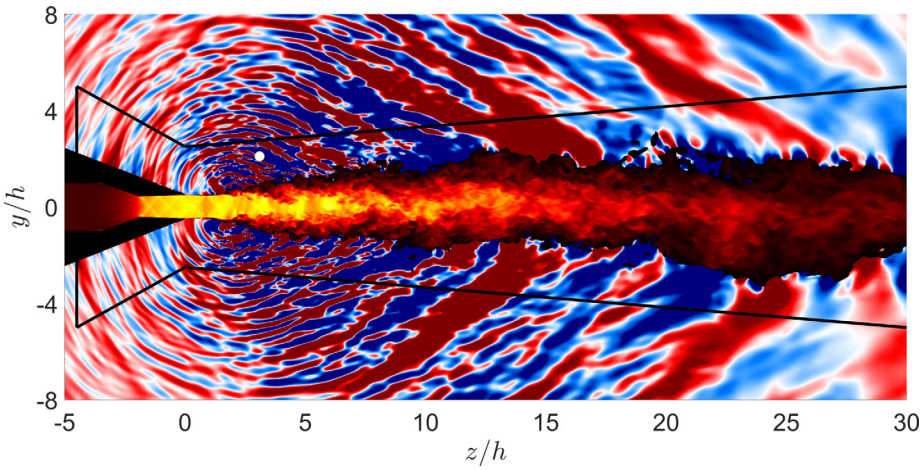

(a) Location of the point probe $(y/h, z/h) = (2.1, 3.1)$. The probe is in white.

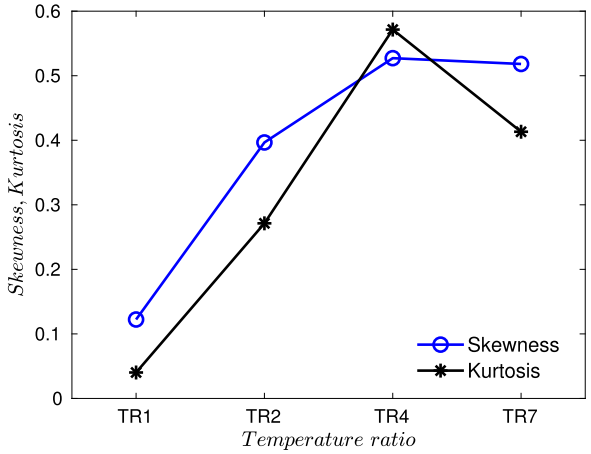

(b) Skewness and kurtosis of p at $(y/h, z/h) = (2.1, 3.1)$.

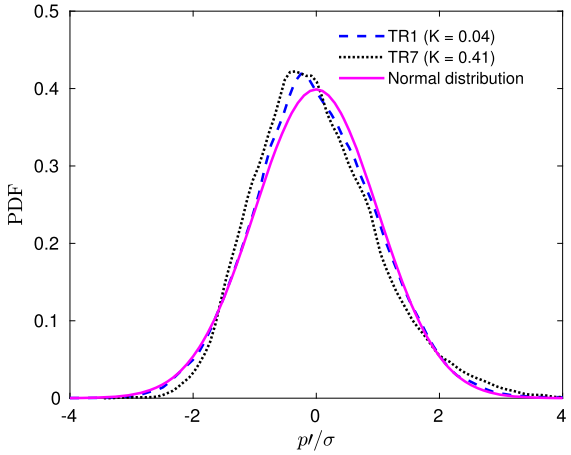

(c) PDF of p' at $(y/h, z/h) = (2.1, 3.1)$.

Fig. 8. Skewness and kurtosis analysis of a point probe at $(y/h, z/h) = (2.1, 3.1)$ along the Mach wave radiation direction.

ponent in the pressure spectra, which supports the idea that this noise component is the MWR.

It seems clear now that how the temperature of the jet plays a role in this scenario. In cold jets, only LTS noise is generated by the subsonic large-scale turbulent structures in the shear layer (see Fig. 12a). In hot jets, MWR appears when the shear layer convection Mach number becomes supersonic. The turbulent structures slow down to subsonic downstream and generate the LTS noise. If the supersonic M_c is just slightly larger than one, the directivities of the MWR and LTS become distinguishable (see Fig. 12b). When the jet is highly heated, the directivity of the MWR and LTS becomes distinguishable (see Fig. 12d). Furthermore, compared with the M_c-dependent MWR directivity, the LTS noise always appears at around 140 $\sim$ 160 degrees without showing significant changes in hot jets.

5.4. Vortex sheet model analysis of the highly-heated jet

In the early works of Tam and Ahuja [58] and Tam and Norum [59], the feedback loop of the impinging jet tones is assumed to be closed by upstream propagating acoustic waves inside the jet. This feedback loop with internal upstream propagating waves has been addressed by Gojon et al. [57] and Bogey and Gojon [60] for planar and round supersonic impinging jets. For the screeching jets, Shen and Tam [61] proposed that the screech feedback cycle may also be closed by neutral acoustic waves propagating upstream. This has recently been confirmed numerically by Gojon et al. [11,34] and experimentally by Edgington-Mitchell et al. [62]. In this section, the vortex sheet model for a rectangular jet [59] is used to analyze whether the upstream-propagating waves exist in the current highly-heated jet and whether they are responsible for the screech tone observed in our LES results.

In rectangular jets, the dispersion relations for wavenumber k and angular frequency ω provided by Tam and Norum [59] are as follows:

$$\frac{\left[\left(\omega - u_j k\right)^2 / a_j^2 - k^2\right]^{1/2} \rho_\infty \omega^2}{\left(k^2 - \omega^2 / a_\infty^2\right)^{1/2} \rho_j \left(\omega - u_j k\right)^2} + \tan\left\{\left[\frac{\left(\omega - u_j k\right)^2}{a_j^2} - k^2\right]^{1/2} h_j/2\right\} = 0 \tag{6}$$

for antisymmetric modes, and

$$\frac{\left[\left(\omega - u_j k\right)^2 / a_j^2 - k^2\right]^{1/2} \rho_\infty \omega^2}{\left(k^2 - \omega^2 / a_\infty^2\right)^{1/2} \rho_j \left(\omega - u_j k\right)^2} - \cot\left\{\left[\frac{\left(\omega - u_j k\right)^2}{a_j^2} - k^2\right]^{1/2} h_j/2\right\} = 0 \tag{7}$$

for symmetric modes. In the dispersion relations, the information of the ideally expanded jets are used, where u_j, a_j and h_j are the

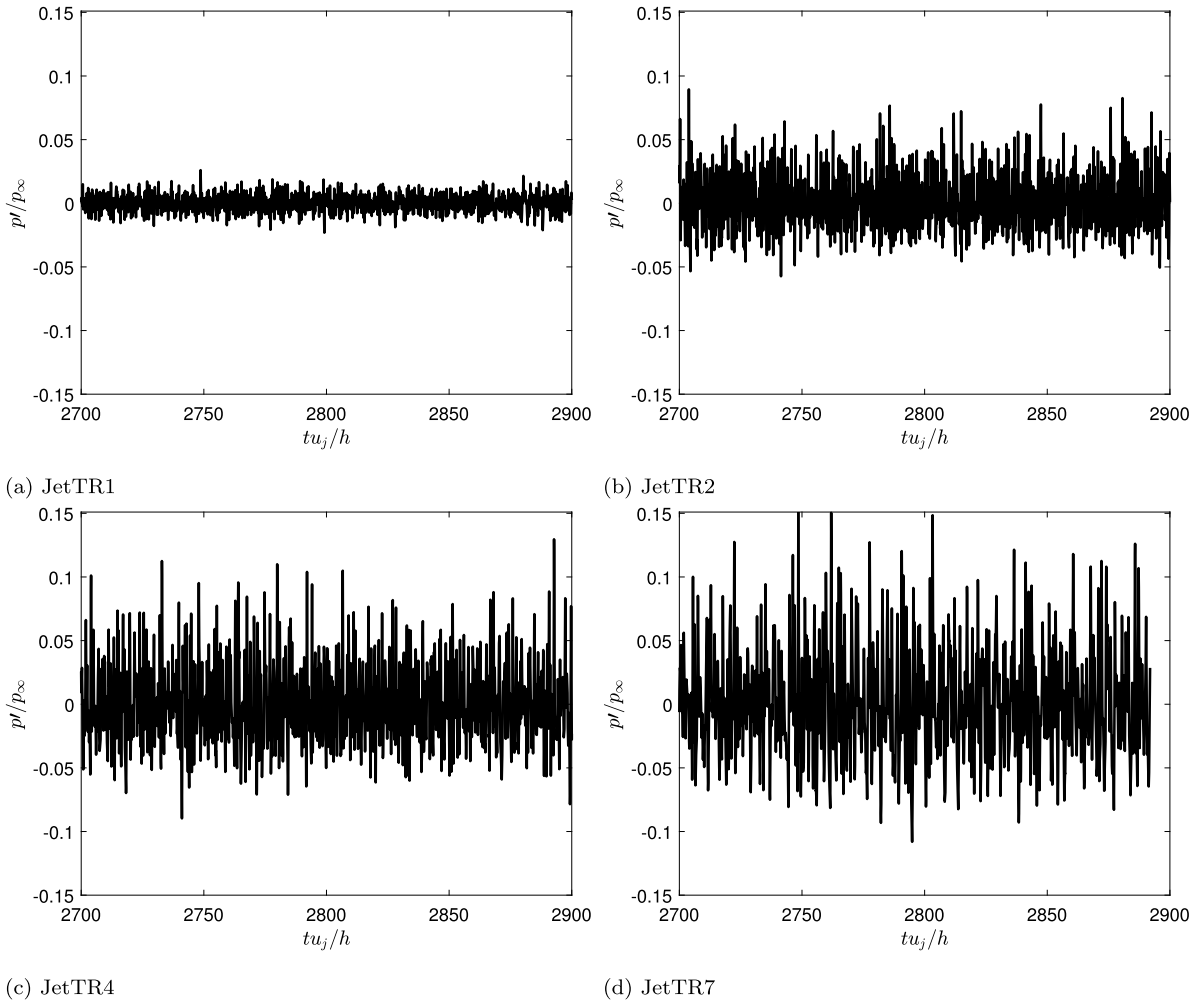

Fig. 9. Pressure fluctuation history at $(y/h, z/h) = (2.1, 3.1)$ for JetTR1 to JetTR7.

jet velocity, speed of sound, and the height of the jet in the ideally expanded condition. h_j is computed based on the work of Tam [50]. a_∞ and ρ_∞ are the ambient speed of sound and ambient density. To be consistent with Eqs. (6) and (7), a Strouhal number based on h_j can be defined as: $St_{hj} = fh_j/u_j = St \times h_j/D_{eq}$. Therefore, the screech Strouhal number $St_{screech} = 0.25$ previously observed in the highly-heated jet JetTR7 can be expressed as $St_{hj} = 0.152$ using the above formula.

The solutions of the dispersion relations in Eqs. (6) and (7) are shown by the solid lines in Fig. 14 as functions of St_{hj} and the normalized wave number. Both symmetric modes and antisymmetric modes are represented and they are marked by the symbol S and A respectively. Based on Tam and Norum [59], the upstream propagating wave modes have a negative group velocity and a negative slope in the $\omega - k$ plane. These waves with a negative slope can be clearly observed in the solid curved lines as shown in Fig. 14. Furthermore, upstream-propagating waves can only exist in a certain range of frequency: the upper limit corresponds to the maximum St_{hj} where $dSt_{hj}/dk = 0$ and the lower limit is determined by the upstream propagating acoustic waves with the group velocity of $-a_\infty$. A round circle is added at the end of each line to indicate the lower limit of each mode.

A space-time Fourier transform is applied to the pressure fluctuation data in the minor axis plane between $z/h = 0$ and $z/h = 10$, aiming to detect any possible upstream-propagating waves in the current highly-heated jet. The frequency-wavenumber spectra contours obtained at different positions are shown in Fig. 14, including one near the jet center-line at $y = 0.1h$, one inside the jet at $y = 0.25h$, and one along the jet shear layer at $y = 0.5h$. By comparing the contours calculated from the LES data with the solid lines obtained from the theoretical dispersion relations, the patterns match with the solutions well. In particular, the upstream-propagating waves with a negative group velocity are visible in the contours too. Near the jet center-line at $y = 0.1h$, the theoretical curves of $A1$ and $S1$ are slightly below the pattern calculated from the LES data. Similar features can be found for the $S1$ mode at $y = 0.25h$ and $y = 0.5h$. This discrepancy may be due to the usage of ideally infinite-thin vortex sheet model and due to the shock wave oscillations in the LES calculations [34]. The magnitudes of detected symmetric mode $S1$ shown in Fig. 14 have a trend to decrease from the location at $y = 0.1h$ towards the jet shear layer $y = 0.5h$. However, the antisymmetric mode $A1$ is maximum at $y = 0.25h$ and its magnitude decays towards both the jet axis and shear layer. This behavior is consistent with the eigenfunction distributions of the neutral acoustic waves provided by Tam and Ahuja [58].

According to Fig. 14(c) and (e), the observed screech Strouhal number $St_{hj} = 0.152$ in the current highly-heated jet falls in the frequency range of antisymmetric mode $A1$. This indicates that at this screech frequency, upstream-propagating neutral acoustic waves exist inside the jet and the oscillation mode is antisymmetric. Furthermore, as the St_{hj} is also close to the lower limit of the neutral wave mode $A1$, that means the neutral waves travel upstream with a group speed close to the speed of sound.

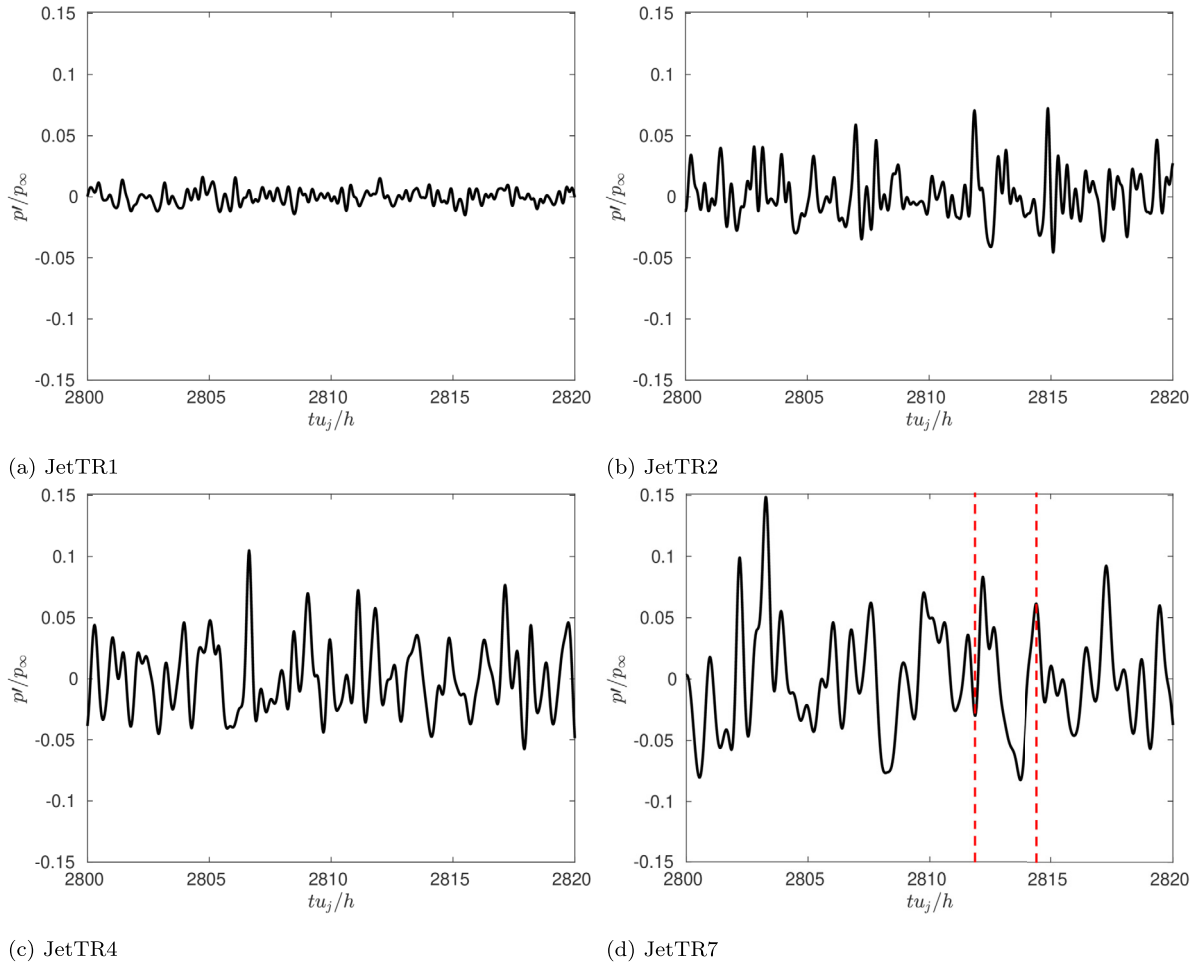

Fig. 10. Zoomed-in pressure wave forms at $(y/h, z/h) = (2.1, 3.1)$ for JetTR1 to JetTR7.

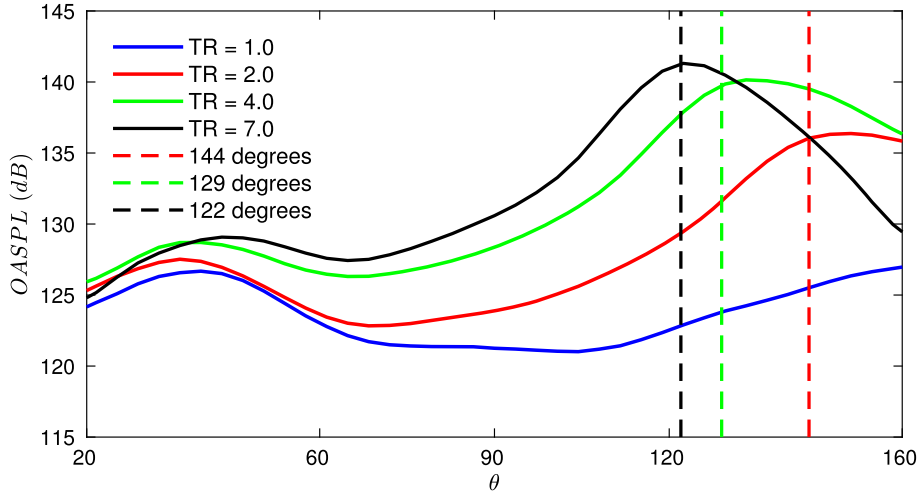

Fig. 11. OASPL at $40D_{eq}$ as function of the angle θ with respect to the upstream direction. The vertical dash lines show the estimated Mach wave radiation angles based on the convection Mach numbers.

To visualize the upstream-propagating waves predicted by the vortex sheet model as discussed above, the LES results are re-examined. Dilatation is computed and shown in Fig. 15. From Figs. 15a to 15i, nines consecutive sampled time snapshots at an interval of $1/8T$ in the nozzle lip region in the minor axis plane are presented, where T is the period of the screech noise and is defined as $T = 1/f_{screech}$. A strong shock and expansion waves structure represented by the dark blue and dark red colors can be seen in the plots. The internally reflected shock waves hit at a location slightly inside the nozzle lip (at $z/h = 0$) and another set of shock waves are generated at the nozzle lip (the jet is over-expanded). The two sets of shock waves merge together and form the first the shock cell at around $z/h = 0.7$. Between the nozzle lip and the first shock cell, the upstream propagating wave indicated

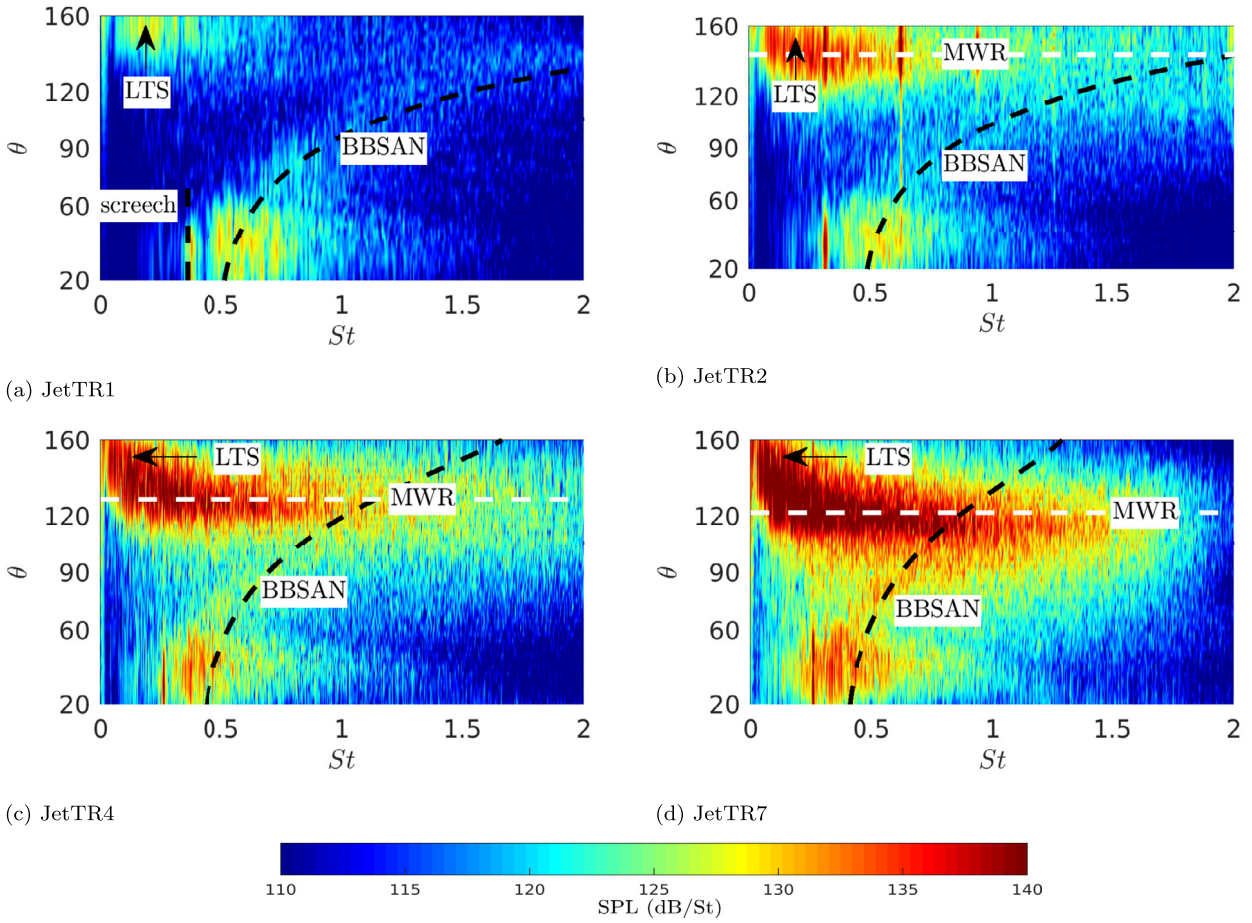

Fig. 12. Far field sound pressure spectra at $40D_{eq}$ as functions of the Strouhal number and the angle θ.

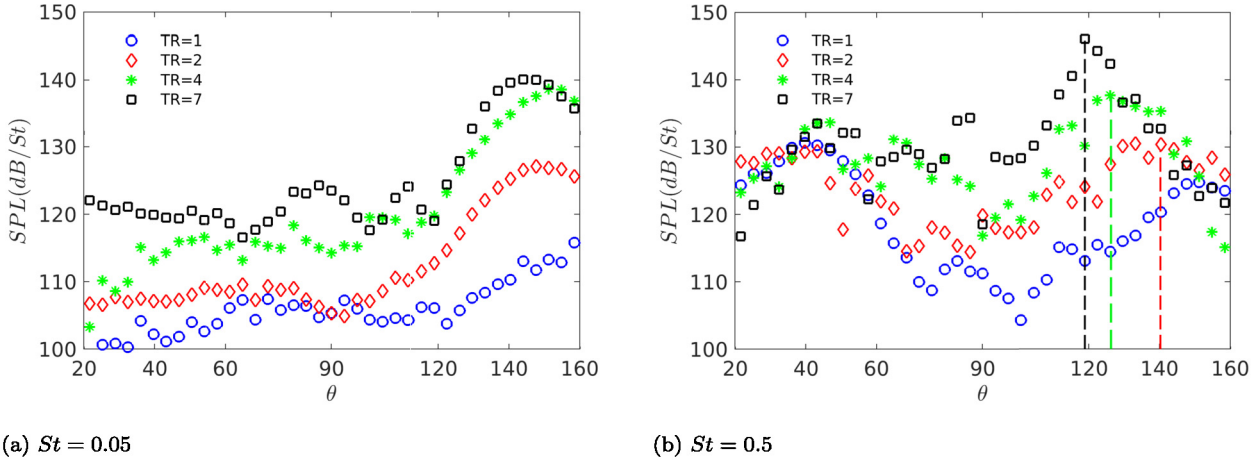

Fig. 13. Far field sound pressure levels at individual Strouhal numbers extracted from Fig. 12: (a) low-frequency $St = 0.05$ and (b) high-frequency $St = 0.5$. Dash lines in b) correspond to the MWR angles.

by the white arrow can be observed. These results confirm the existence of the upstream propagating wave inside the highly-heated supersonic jet.

6. Conclusion

Transitional rectangular supersonic jets with a fixed nozzle pressure ratio but different temperature ratios (from a cold jet TR 1.0 to a highly-heated one TR 7.0) have been numerically studied by implicit LES and FW-H acoustic analogy. When heated to high temperatures, the jet shows an increased velocity and acoustic Mach number. Shear layers in the rectangular jet develop differently along the minor and major axis planes as observed in experimental works [3]. It exhibits a larger convection velocity in the minor axis plane than the major axis plane does. The convection Mach number of the shear layer is found to increase from subsonic to supersonic with the increasing jet temperature. Those trends are consistent with the findings reported in highly-heated round jets [36] and moderately-heated rectangular jets [34]. Nevertheless, compared with the cold jet, the most heated jet TR 7.0

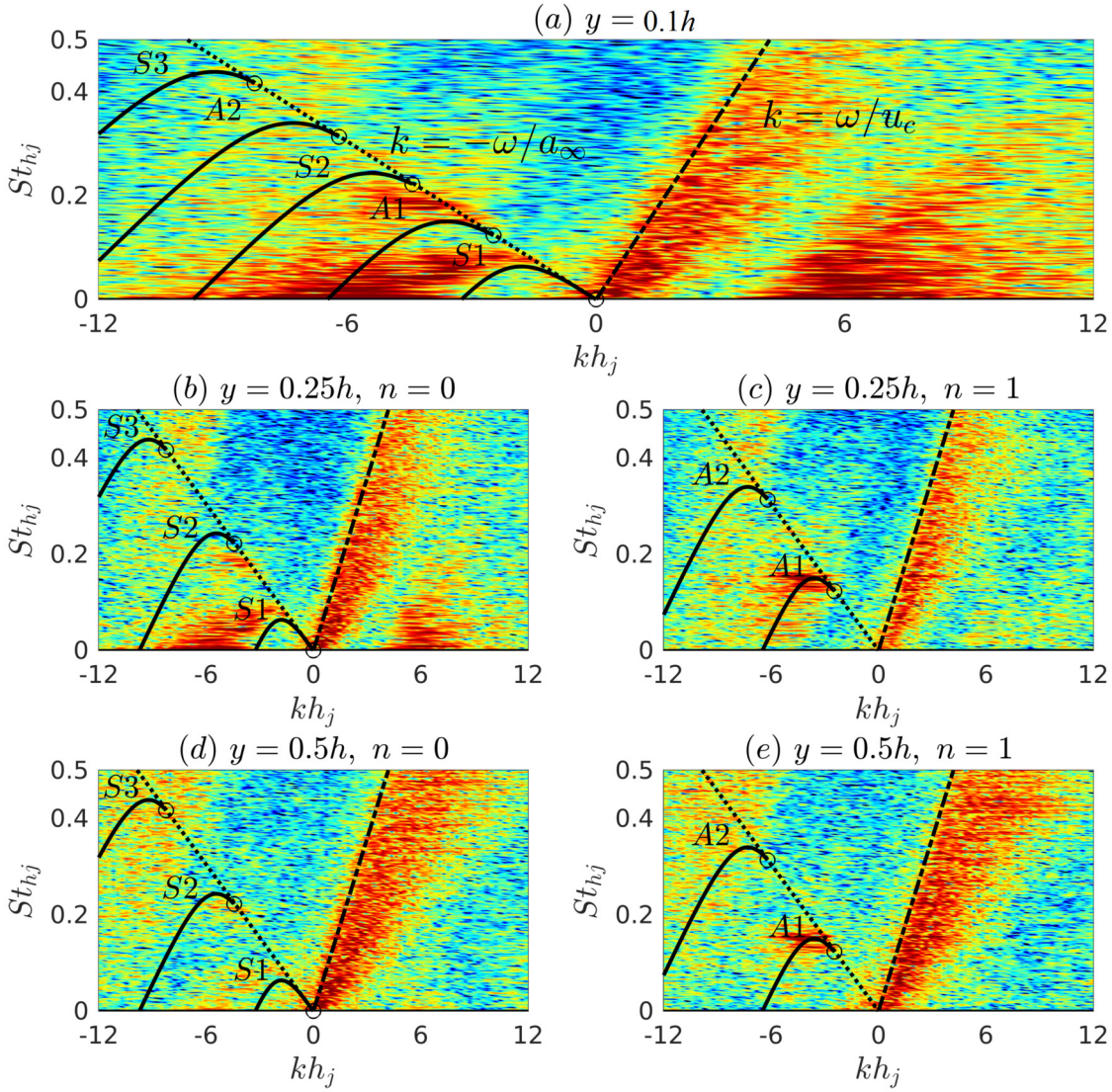

Fig. 14. Frequency-wavenumber spectra of pressure fluctuations of the JetTR7 with an NPR 3.0 and a TR 7.0 at (a) $y = 0.1h$, (b, c) $y = 0.25h$, and (d, e) $y = 0.5h$ for the planar mode $n = 0$ and $n = 1$. The solid lines denote the solutions of the dispersion relations: the symmetric modes (marked by S) and the antisymmetric modes (marked by A). The round circle represents the lower limits of the modes.

in the present study exhibits significant differences in flow fields: (1) the jet Reynolds number decreases by about an order of magnitude which leads to a 30% shorter jet potential core length and fewer shock cells; (2) the jet acoustic Mach number is amplified by about 3 times; (3) the shear layer convection Mach number is increased by about 2 times.

Near-field acoustic results reveal that the OASPL is amplified at all directions with the increasing temperature. Except for the cold jet TR 1.0, Mach wave radiations exist in both the minor and major axis planes for heated jets. When the jet is heated to high temperatures, the Mach wave radiation becomes the dominant noise component. This is consistent with the finding reported in moderately heated transitional round supersonic jets [14], because the laminar shear layers of transitional jets roll and form large turbulent structures during the transition, which therefore yields stronger Mach wave radiation than a fully turbulent jet does. The intensity of the screech noise is found to be increasing with the temperature although the opposite trend is reported in experiments [22]. This disagreement is believed to be caused by the transitional nature of jets in the present study. Analysis of pressure skewness and kurtosis factors indicates the existence of the crackle noise component and non-linear propagation effects in TR 4.0 and TR 7.0. In the far-field acoustics, the evidence is provided that for the highly-heated jet JetTR7, a dominant lower-frequency noise component (St of 0.05) propagates to 140 ∼ 160 degrees, while a higher-frequency component (St of 0.5) propagates to a different angle at about 120 degrees. These features have been associated with the large turbulent structure noise (at 140 ∼ 160 degrees) and with the Mach wave radiation (radiating at about 120 degrees), respectively. It has to be noted that Tam et al. [38] reported a similar double-peaks pattern associated with F-22A data characterized by one SPL spectra peak at around 150 degrees and the other peak at around 120 degrees.

Through the vortex sheet model analysis for TR 7.0, upstream-propagating neutral waves, recently observed numerically by Gojon et al. [11,34] and experimentally by Edgington-Mitchell et al. [62] in low-temperature screeching jets are also detected in the current highly-heated jets. The antisymmetric neutral upstream-propagating wave is found to be responsible for the screech tone, explaining the oscillation mode associated to the screech frequency. The existence of the upstream propagating wave inside the current highly-heated jet is also visualized in the LES flow fields.

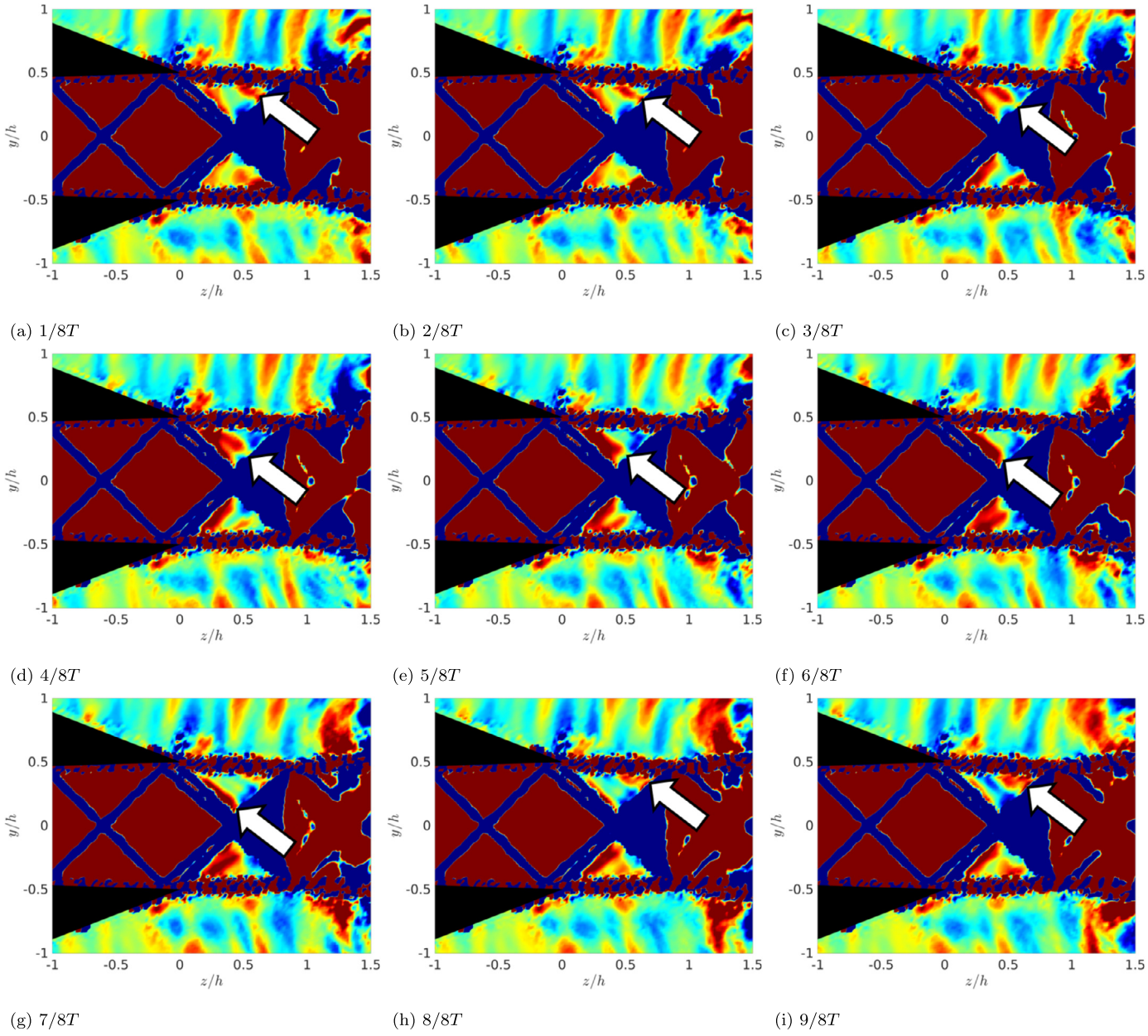

Fig. 15. Instantaneous dilatation contours to show the upstream propagating waves inside the highly-heated jet JetTR7 at nine consecutive times from (a) to (i). Dark blue color denotes shock waves, dark red color represents expansion regions. The nozzle tips are in black. White arrows indicate the location of the upstream propagating wave represented by the red color. (For interpretation of the colors in the figure(s), the reader is referred to the web version of this article.)

Declaration of competing interest

The authors declare that they have no known competing financial interests or personal relationships that could have appeared to influence the work reported in this paper.

Acknowledgements

The computations were performed on resources provided by the Swedish National Infrastructure for Computing (SNIC) at PDC Centre for High-Performance Computing (PDC-HPC). The authors would like to thank Stefan Wallin at KTH for the assistance of the code modification and implementations. Florian Baier, Aatresh Karnam and Ephraim Gutmark at the University of Cincinnati are also acknowledged for sharing the experimental data and discussion.

References

[1] P. Hiley, H. Wallacet, D. Booz, Nonaxisymmetric nozzles installed in advanced fighter aircraft, J. Aircr. 13 (12) (1976) 1000–1006.
[2] K. Viswanath, R. Johnson, A. Corrigan, K. Kailasanath, P. Mora, F. Baier, E. Gutmark, Flow statistics and noise of ideally expanded supersonic rectangular and circular jets, AIAA J. 55 (10) (2017) 1–15.
[3] E. Gutmark, F. Grinstein, Flow control with noncircular jets, Annu. Rev. Fluid Mech. 31 (1) (1999) 239–272.
[4] M.B. Gerdroodbary, Modern techniques for fuel injections, in: Scramjets: Fuel Mixing and Injection Systems, 2020, pp. 205–213.
[5] D. Casalino, F. Diozzi, R. Sannino, A. Paonessa, Aircraft noise reduction technologies: a bibliographic review, Aerosp. Sci. Technol. 12 (1) (2008) 1–17.
[6] X. Wei, L. Chua, Z. Lu, H. Lim, R. Mariani, Y. Cui, T. New, Experimental investigations on screech mitigation and amplification by bevelled and double-bevelled nozzles, Aerosp. Sci. Technol. (2020) 105782.
[7] P. Balakrishnan, K. Srinivasan, Influence of swirl number on jet noise reduction using flat vane swirlers, Aerosp. Sci. Technol. 73 (2018) 256–268.
[8] C.K. Tam, Supersonic jet noise, Annu. Rev. Fluid Mech. 27 (1) (1995) 17–43.
[9] C. Bailly, K. Fujii, High-speed jet noise, Mech. Eng. Rev. 3 (1) (2016) 15–00496.

[10] R. Gojon, C. Bogey, Numerical study of the flow and the near acoustic fields of an underexpanded round free jet generating two screech tones, Int. J. Aeroacoust. 16 (7–8) (2017) 603–625.
[11] R. Gojon, C. Bogey, M. Mihaescu, Oscillation modes in screeching jets, AIAA J. 56 (7) (2018) 2918–2924.
[12] C. Bogey, C. Bailly, Influence of nozzle-exit boundary-layer conditions on the flow and acoustic fields of initially laminar jets, J. Fluid Mech. 663 (2010) 507–538.
[13] T. Nonomura, K. Fujii, Effects of inflow shear layer parameters on a transitional supersonic jet with a moderate Reynolds number, in: 19th AIAA/CEAS Aeroacoustics Conference, 2013, p. 2237.
[14] T. Nonomura, H. Nakano, Y. Ozawa, D. Terakado, M. Yamamoto, K. Fujii, A. Oyama, Large eddy simulation of acoustic waves generated from a hot supersonic jet, Shock Waves (2019) 1–22.
[15] M. Harper-Bourne, M.J. Fisher, The noise from shock waves in supersonic jets, in: AGARD-CP-131, 1973.
[16] A. Powell, On the mechanism of choked jet noise, Proc. Phys. Soc. B 66 (12) (1953) 1039–1057.
[17] A. Powell, The noise of choked jets, J. Acoust. Soc. Am. 25 (3) (1953) 385–389.
[18] J.B. Freund, P. Moin, Jet mixing enhancement by high-amplitude fluidic actuation, AIAA J. 38 (10) (2000) 1863–1870.
[19] T. Castelain, M. Sunyach, D. Juvé, J.-C. Bera, Jet-noise reduction by impinging microjets: an acoustic investigation testing microjet parameters, AIAA J. 46 (5) (2008) 1081–1087.
[20] N. Heeb, J. Kastner, E. Gutmark, K. Kailasanath, Supersonic jet noise reduction by chevrons and fluidic injection, Int. J. Aeroacoust. 12 (7–8) (2013) 679–697.
[21] N. Heeb, P. Mora, E. Gutmark, K. Kailasanath, Investigation of the noise from a rectangular supersonic jet, in: AIAA Paper 2013-2239, 2013.
[22] P. Mora, F. Baier, K. Kailasanath, E.J. Gutmark, Acoustics from a rectangular supersonic nozzle exhausting over a flat surface, J. Acoust. Soc. Am. 140 (6) (2016) 4130–4141.
[23] F. Baier, A. Karnam, E.J. Gutmark, K. Kailasanath, High temperature supersonic flow measurements of a rectangular jet exhausting over a flat surface, AIAA Paper, 2018-0012, 2018.
[24] A. Karnam, F. Baier, E.J. Gutmark, K. Kailasanath, Flow measurement and acoustic investigation of high temperature rectangular jets, AIAA Paper, 2018-0260, 2018.
[25] C.K. Tam, A. Ganesan, Modified $k-\varepsilon$ turbulence model for calculating hot jet mean flows and noise, AIAA J. 42 (1) (2004) 26–34.
[26] C.K. Tam, N.N. Pastouchenko, K. Viswanathan, Fine-scale turbulence noise from hot jets, AIAA J. 43 (8) (2005) 1675–1683.
[27] R.F. Davey, A. Roshko, The effect of a density difference on shear-layer instability, J. Fluid Mech. 53 (3) (1972) 523–543.
[28] E. Gutmark, K. Schadow, K. Wilson, Effect of convective Mach number on mixing of coaxial circular and rectangular jets, Phys. Fluids A, Fluid Dyn. 3 (1) (1991) 29–36.
[29] M. Doty, D.K. McLaughlin, Two-point correlations of density gradient fluctuations in high speed jets using optical deflectometry, in: AIAA Paper 2002-0367, 2002.
[30] K. Viswanathan, Aeroacoustics of hot jets, J. Fluid Mech. 516 (2004) 39–82.
[31] N. De Cacqueray, C. Bogey, Noise of an overexpanded Mach 3.3 jet: non-linear propagation effects and correlations with flow, Int. J. Aeroacoust. 13 (7–8) (2014) 607–632.
[32] A. Langenais, F. Vuillot, J. Troyes, C. Bailly, Numerical investigation of the noise generated by a rocket engine at lift-off conditions using a two-way coupled cfd-caa method, in: AIAA Paper 2017-3212, 2017.
[33] R. Gojon, F. Baier, E. Gutmark, M. Mihaescu, Temperature effects on the aerodynamic and acoustic fields of a rectangular supersonic jet, in: AIAA Paper 2017-0002, 2017.
[34] R. Gojon, E. Gutmark, M. Mihaescu, Antisymmetric oscillation modes in rectangular screeching jets, AIAA J. 57 (8) (2019) 3422–3441.
[35] J. Liu, A. Corrigan, K. Kailasanath, B. Taylor, Impact of the specific heat ratio on noise generation in a high-temperature supersonic jet, in: AIAA Paper 2016-2125, 2016.
[36] J. Liu, A.T. Corrigan, K. Kailasanath, E.J. Gutmark, Effects of temperature on noise generation in supersonic jets, in: AIAA Paper 2016-2937, 2016.
[37] J. Liu, K. Kailasanath, E.J. Gutmark, Similarity spectra analysis in highly heated supersonic jets using large-eddy simulations, in: AIAA Paper 2017-0926, 2017.
[38] C.K. Tam, S.A. Parrish, Noise of high-performance aircraft at afterburner, J. Sound Vib. 352 (2015) 103–128.
[39] R. Gojon, E. Gutmark, M. Mihaescu, On the response of a rectangular supersonic jet to a near-field located parallel flat plate, in: AIAA Paper 2017-3018, 2017.
[40] P. Mora, F. Baier, E.J. Gutmark, K. Kailasanath, Acoustics from a rectangular c-d nozzle exhausting over a flat surface, in: AIAA Paper 2016-1884, 2016.
[41] F. Baier, P. Mora, E.J. Gutmark, K. Kailasanath, Flow measurements from a supersonic rectangular nozzle exhausting over a flat surface, in: AIAA Paper 2017-0932, 2017.
[42] S. Chen, R. Gojon, M. Mihaescu, High-temperature effects on aerodynamic and acoustic characteristics of a rectangular supersonic jet, in: AIAA Paper, 2018-3303, 2018.
[43] Chemical equilibrium with applications, https://www.grc.nasa.gov/www/CEAWeb. (Accessed November 2017), Online.
[44] W. Sutherland, Lii. the viscosity of gases and molecular force, The London, Edinburgh, and Dublin Philosophical Magazine and Journal of Science 36 (223) (1893) 507–531.
[45] P. Eliasson, Edge: a Navier-Stokes solver for unstructured grids, 2001.
[46] B. Semlitsch, D.R. Cuppoletti, E.J. Gutmark, M. Mihaescu, Transforming the shock pattern of supersonic jets using fluidic injection, AIAA J. (2019) 1–11.
[47] L.G. Margolin, W.J. Rider, A rationale for implicit turbulence modelling, Int. J. Numer. Methods Fluids 39 (9) (2002) 821–841.
[48] C. Fureby, F. Grinstein, Monotonically integrated large eddy simulation of free shear flows, AIAA J. 37 (5) (1999) 544–556.
[49] A. Jameson, W. Schmidt, E. Turkel, Numerical solution of the Euler equations by finite volume methods using Runge-Kutta time-stepping schemes, in: AIAA Paper 1981-1259, 1981.
[50] C. Tam, The shock-cell structures and screech tone frequencies of rectangular and non-axisymmetric supersonic jets, J. Sound Vib. 121 (1) (1988) 135–147.
[51] H. Oertel, Kinematics of Mach waves inside and outside supersonic jets, in: Recent Developments in Theoretical and Experimental Fluid Mechanics, Springer, 1979, pp. 121–136.
[52] J.F. Williams, J. Simson, V. Virchis, Crackle: an annoying component of jet noise, J. Fluid Mech. 71 (2) (1975) 251–271.
[53] J.W. Nichols, S.K. Lele, F.E. Ham, S. Martens, J.T. Spyropoulos, Crackle noise in heated supersonic jets, J. Eng. Gas Turbines Power 135 (5) (2013) 051202.
[54] A. Krothapalli, L. Venkatakrishnan, L. Lourenco, Crackle: a dominant component of supersonic jet mixing noise, in: AIAA Paper 2000-2024, 2000.
[55] A. Krothapalli, V. Arakeri, B. Greska, Mach wave radiation: a review and an extension, in: AIAA Paper 2003-1200, 2003.
[56] P. Mora, N. Heeb, J. Kastner, E.J. Gutmark, K. Kailasanath, Impact of heat on the pressure skewness and kurtosis in supersonic jets, AIAA J. 52 (4) (2014) 777–787.
[57] R. Gojon, C. Bogey, O. Marsden, Investigation of tone generation in ideally expanded supersonic planar impinging jets using large-eddy simulation, J. Fluid Mech. 808 (2016) 90–115.
[58] C.K. Tam, K. Ahuja, Theoretical model of discrete tone generation by impinging jets, J. Fluid Mech. 214 (1990) 67–87.
[59] C.K. Tam, T.D. Norum, Impingement tones of large aspect ratio supersonic rectangular jets, AIAA J. 30 (2) (1992) 304–311.
[60] C. Bogey, R. Gojon, Feedback loop and upwind-propagating waves in ideally expanded supersonic impinging round jets, J. Fluid Mech. 823 (2017) 562–591.
[61] H. Shen, C.K.W. Tam, Three-dimensional numerical simulation of the jet screech phenomenon, AIAA J. 40 (1) (2002) 33–41.
[62] D. Edgington-Mitchell, V. Jaunet, P. Jordan, A. Towne, J. Soria, D. Honnery, Upstream-travelling acoustic jet modes as a closure mechanism for screech, J. Fluid Mech. 855 (2018).